

***Ab-initio* investigation of hot electron transfer in CO₂ plasmonic photocatalysis in presence of hydroxyl adsorbate**

Zelio Fusco¹, Dirk Koenig², Sean C. Smith², Fiona Jean Beck¹

¹Renewable fuel group, School of Engineering, College of Engineering, Computing and Cybernetics, The Australian National University, Canberra, ACT 2601, Australia

²Integrated Materials Design Lab, The Australian National University, Canberra, ACT 2601, Australia

Abstract

Photoreduction of carbon dioxide (CO₂) on plasmonic structures is of great interest in photocatalysis to aid selectivity. While species commonly found in reaction environments and associated intermediates can steer the reaction down different pathways by altering the potential energy landscape of the system, they are often not addressed when designing efficient plasmonic catalysts. Here, we perform an atomistic study of the effect of the hydroxyl group (OH) on CO₂ activation and hot electron generation and transfer using first-principle calculations. We show that the presence of OH is essential in breaking the linear symmetry of CO₂, which leads to a charge redistribution and a decrease in the O=C=O angle to 134°, thereby activating CO₂. Analysis of the partial density of states (pDOS) demonstrates that the OH group mediates the orbital hybridization between Au and CO₂ resulting in more accessible states, thus facilitating charge transfer. By employing time-dependent density functional theory (TDDFT), we quantify the fraction of hot electrons directly generated into hybridized molecular states at resonance, demonstrating a broader energy distribution and a 11% increase in charge-transfer in the presence of OH groups. We further show that the spectral overlap between excitation energy and plasmon resonance plays a critical role in efficiently modulating electron transfer processes. These findings contribute to the mechanistic understanding of plasmon-mediated reactions and demonstrate the importance of co-adsorbed species in tailoring the electron transfer processes, opening new avenues for enhancing selectivity.

Introduction

Subwavelength metallic nanoparticles that support plasmonic resonances represent a versatile platform for nanoscale light manipulation. These structures hold great potential in nanophotonic applications that benefit from enhanced near-field light-matter interactions, such as plasmon-enhanced biosensing[1-3], surface-enhanced Raman scattering[4, 5] and photocatalysis[6-8]. Harnessing the hot electrons (HE)[9] generated by the non-radiative decay of illuminated metal nanoparticles before they thermalise is an attractive way to initiate and selectively drive chemical reactions[10-13], and has recently attracted significant interest in the heterogeneous catalysis community[14-18]. Hot electrons can be rapidly transferred to orbitals of nearby molecules, thereby driving catalytic chemical reactions. The energy and momentum distribution of the hot carriers depend on multiple factors, including material, particle morphology, crystal orientation, defects and environs[19, 20], influencing many aspects of heterogeneous catalysis, including reaction rate, selectivity, turnover frequency, yield, and reaction order[21]. To date, the significant role of HEs provided by photoexcited plasmons have been attributed to many reactions, including water splitting[22], bond cleavage[23] or formation[24], and carbon dioxide reduction[25].

Once generated, HEs can be transferred to nearby molecules directly or indirectly[26, 27]. In the former process, HEs are directly excited from the metal into unoccupied molecular orbitals of interacting acceptor adsorbates. The latter process comprises HEs generated within metal nanoparticles, subsequently being scattered to empty states of surface-adsorbed molecules with suitable overlaps in energy and momentum distribution. The direct injection of HEs is a faster and more efficient process compared to the indirect transfer[28], and offers great potential for enabling

high selectivities to adsorbed chemical species and their reaction paths[28-30]. High selectivities can be achieved by precisely tuning the plasmon resonance and the energy distribution of HEs to align with targeted unoccupied adsorbate states, thereby selectively promoting a specific reaction pathway[6, 17, 30]. The design and engineering of the optoelectronic properties of plasmonic architectures is thus important in particular to achieve selectivity in multiproduct reactions such as CO₂ reduction[31].

In the context of plasmon-enabled chemical transformations, reactions pathways and activation energies are often being investigated with ground-state density functional theory (DFT) methods[32-35]. Although these analyses provide important information on the systems and contribute to the understanding of the action mechanisms, they cannot accurately capture the physics of excited-states and the dynamics of the photogenerated hot carriers. Instead, time-dependent DFT (TDDFT) approaches have been increasingly employed to shed light on plasmon dynamics and hot carrier generation[36-38] by providing atomic-scale insights into excitation and transfer processes of electrons. In particular Rossi et al. have developed a real-time TDDFT methodology to study the dynamics of plasmon-molecules systems[39-43], demonstrating that the generated HEs have an energetic and spatial distribution that depends on the atomic structure, with lower-coordinated atoms exhibiting a higher proportion of HEs[41]. These can be directly transferred to adjacent semiconductors[40] or molecules[29, 42], even when the molecule is not chemisorbed to the plasmonic nanoparticle[42]: using Ag-CO as a model system, Fojt *et al.* demonstrated that HEs can be directly generated on the molecule at distances up to 5Å.

We extend the approach of Rossi et al. to investigate the energy required to activate carbon dioxide (CO₂) on a small Au cluster in the presence of co-adsorbed environmental species and probe the carrier dynamics. It is widely accepted that the reaction environment and intermediate species can steer the reaction pathway[44-46] by altering the potential energy landscape of the chemical transformation. However, a mechanistic study of the effect of intermediate adsorbates on the HE generation and transfer in CO₂ reduction is still missing. Here, we focus specifically on the role of adsorbed hydroxyl groups, as they take part in the CO₂RR and are crucial for enhanced stability, activity and selectivity[47-49]. By using TDDFT calculations, we study the HE transfer process as a function of the distance, excitation frequency and an increasingly non-monochromatic frequency distribution, extending the fundamental understanding of HE transfer across nanoparticle-molecule interfaces and their impact on the overall CO₂ reduction reaction.

Results and Discussion

System description

We consider CO₂ as a reactant species because its reduction is of significant industrial and societal importance: artificial synthesis of hydrocarbons and alcohols from CO₂, using water to provide hydrogen and sunlight to drive the reaction, has the potential to provide renewable fuels and chemicals at scale[17, 50]. A considerable challenge in converting CO₂ into organic products lies in its activation, due to the notably high reaction barrier linked to the initial electron transfer (-1.9V vs standard hydrogen electrode). Adsorption of CO₂ on catalytic surfaces forms partially charged CO₂^{δ-} species which –due to charge redistribution– results in a change in the O=C=O bond angle and leads to a bent configuration[51, 52], as shown in Fig. 1a. As a consequence, the lowest unoccupied molecular orbital (LUMO) shifts to lower energies, reducing the energy barrier required for electron transfer and promoting a CO₂ reduction reaction[53].

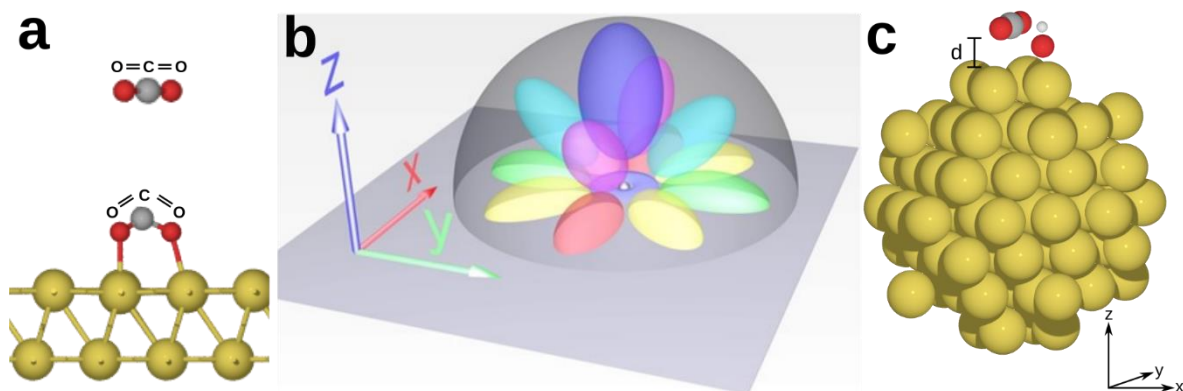


Figure 1. a) Activation of CO_2 on a catalytic surface. The free molecule has a linear configuration with a $\text{O}=\text{C}=\text{O}$ bond angle of 180° ; upon interaction with the surface atoms the bond angle reduces, thus activating CO_2 . b) Spatial scheme of the valence orbitals of a gold atom (bright grey sphere) on the catalytic surface: Colour-coding represents the spherical $6s$ (grey), d_{xy} (yellow), $d_{x^2-y^2}$ (red and green), d_{xz} (purple), d_{yz} (cyan) and d_{z^2} (blue). Colours refer to AO lobes aligned to x -/ y -/ z -axis (red/green/blue), and superimposed colours for bi-axial orientation; xy shown by yellow, xz shown by magenta, and yz shown by cyan. c) Schematic representation of the system analysed in this work, comprising of a Au_{87} cluster with an OH group and CO_2 .

We use gold as a standard plasmonic material because of its unique electronic configuration which allows it to efficiently mediate catalytic reactions[31, 54]. The electronic configuration of Au is shaped considerably by its atomic orbital arrangement. Gold has a $5d^{10}6s^1$ valence orbital configuration which consists of five filled $5d$ atomic orbitals that enable hybridization with various reactant molecules, and a partially filled $6s$ orbital. The five $5d$ orbitals are strongly lobed and are overlaid by the diffused spherical $6s$ orbital which does not hybridize with the $5d$ orbitals. The large nuclear charge of gold leads to a more pronounced nuclear-electron attraction of the valence electron shell: due to relativistic effects, the s -orbitals are found to contract in response to the large nuclear charge, while the d -orbitals are in fact expanded and thus increases their involvement in the chemical and physical properties of gold[55, 56]. These specific atomic orbital lobes allow for various combinations of hybridisation and complex formation with molecular species and ligands, making gold a promising material for catalytic applications and HE transfer. It is worth noting that this versatility may pose challenges to spatial selectivity, as gold can couple with numerous molecular species. However, the resulting higher spatial probability of an electron transfer due to an increased overlap integral of the atomic and/or molecular orbitals involved promotes catalytic reactions. Selectivity for a specific reaction can be achieved by carefully tuning and aligning the energy distribution of HEs with the energy of the lowest unoccupied molecular orbitals (LUMO) of the reactant species[28], as discussed at the end of this section.

Electronic ground state properties

We start by investigating the adsorption and activation of a CO_2 molecule on a Au_{87} cluster in presence and absence of an adsorbed hydroxyl group by performing a structural relaxation. The two model systems are $\text{Au}_{87} + \text{CO}_2$ and $\text{Au}_{87} + \text{OH} + \text{CO}_2$, with the CO_2 initially placed at a varying distance $2 \text{ \AA} < d < 5 \text{ \AA}$ on a bridge-site, as this is the most catalytically active site for CO_2 reduction on gold surfaces[57], while the OH group is adsorbed on an on-top site.

Figure 2a shows the $\text{O}=\text{C}=\text{O}$ bond angle when the systems reached equilibrium (forces < 0.05 eV/atom). In absence of the OH group, CO_2 maintains a linear symmetry with a final equilibrium $\text{O}=\text{C}=\text{O}$ angle which fluctuates around 178° , independent of the distance from the Au cluster (red curve). Contrarily, the presence of OH group perturbs the charge symmetry of the molecule, leading to a structure transformation for $d < 3 \text{ \AA}$. This results in a bent configuration with a final equilibrium $\text{O}=\text{C}=\text{O}$ angle of 133° , in line with previous theoretical reports on activated CO_2 on catalysts surfaces[51, 52]. Similar results are also obtained on periodic gold slabs (see Supporting Information

S1). Simultaneously, as the CO₂ approaches the Au cluster ($d < 3 \text{ \AA}$), a redistribution of the charge density occurs, as can be seen by the different LUMO shapes of the system (Fig. 2b). These results suggest the importance of investigating the effects of co-adsorbed hydroxyl groups – and possibly other environmental species – in the overall activation of CO₂, as well as the role of such species in HE transfer for efficiently driving catalytic processes.

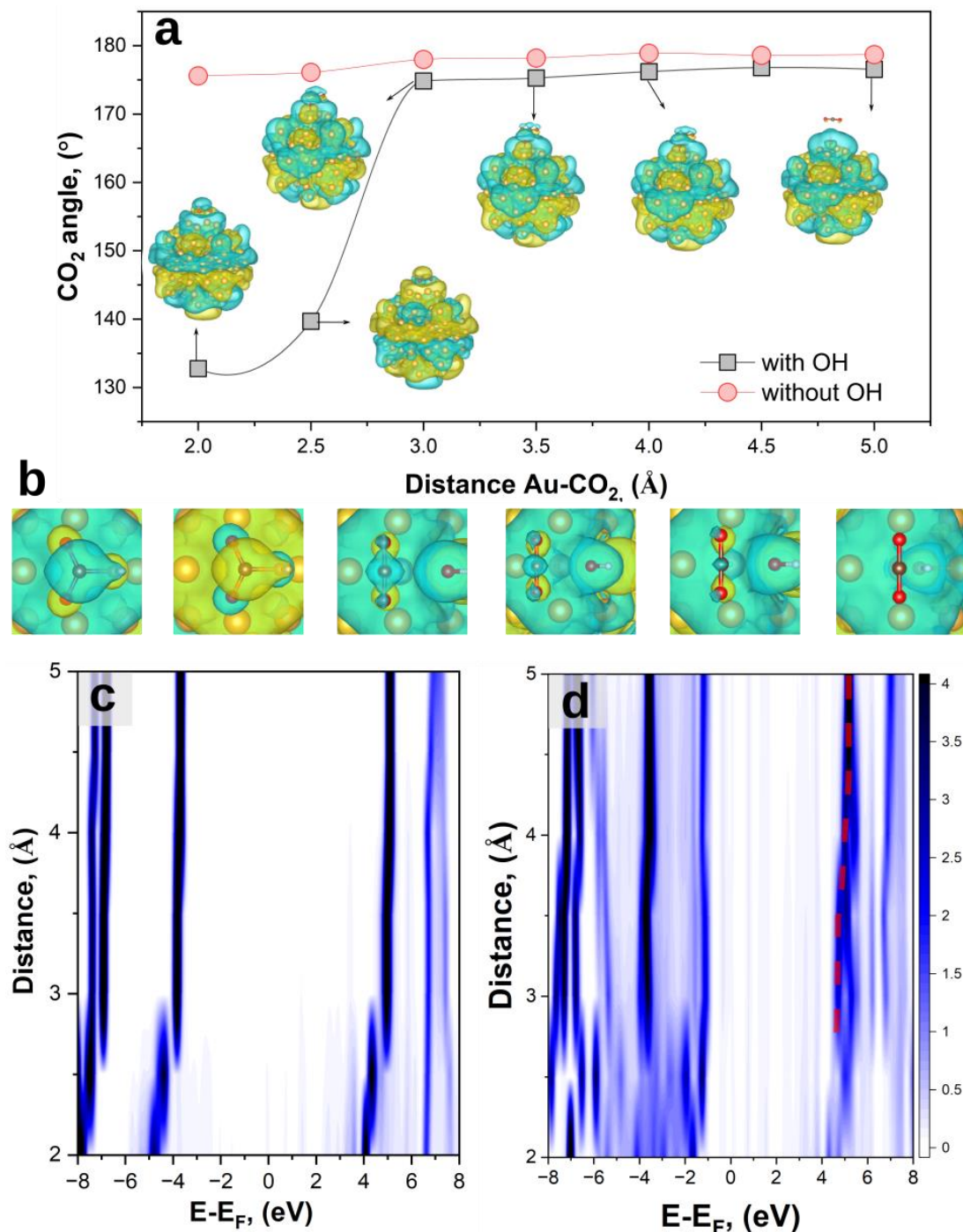


Figure 2. a) CO₂ bond angle as a function of the distance during the adsorption process on Au and Au + OH clusters, red and black curves respectively. The LUMO wave functions of the systems are also shown at a the same isosurface value of 0.05 a.u. b) Magnification of the top-view of the LUMO at the same distances of (a). At a $d = 2.5 \text{ \AA}$, when transitioning from weak to strong hybridization (from 3 \AA to 2.5 \AA), we observe a phase flip in the molecular orbital (MO) lobes. This is due to the spin eigenfunction of the MO changing state, i.e. from spin-up to spin-down. When a phase flip happens, it means that the energy difference between both spin states of the MO is very small ($\leq k_B T$) so that both electrons can swap their spin eigenfunction (spinor) within the MO. The spin-flip occurrence when going from 3 \AA to 2.5 \AA and then back to the original spin configuration shows that one spin configuration of the LUMO has a slightly higher E_{LUMO} compared to the E_{LUMO} at $d = 2 \text{ \AA}$. c, d) Map of the projected density of states as a function of the distance and energy for Au + CO₂ and Au + CO₂ + OH.

When CO₂ approaches the Au and Au + OH clusters, the strength of orbital hybridization increases[42]. This can be demonstrated by analysing the projected density of states (pDOS) of the adsorbed molecules as a function of their distance to the Au surface for the different systems (Fig. 2c, d). At distances $d \gtrsim 4 \text{ \AA}$ for both, Au+CO₂ and Au+OH+CO₂ systems, the pDOS converges to the molecular density of states (DOS) of the isolated molecules. As d decreases, the pDOS eventually splits into several branches due to hybridisation with Au orbitals[42]. The addition of the OH group qualitatively shows a similar trend with a branched pDOS (Fig. 2b), but with an increased number of electronic states. In other words, the OH group mediates the orbital hybridization between Au and CO₂, allowing for more accessible states.

We anticipate that these states are of significant importance for the further HE transfer process[31]; in fact, a HE transfer to the adsorbed molecule requires the presence of acceptor states at suitable energies, i.e. where the pDOS is present[42], thus having more unoccupied levels which can lead to an increase of catalytic efficiency.

Additionally, this adsorption process is also accompanied by a shift towards a lower binding energy of the LUMO, decreasing from $\sim 4.9 \text{ eV}$ ($d \gtrsim 4 \text{ \AA}$) to $\sim 4.6 \text{ eV}$ ($d \sim 3.5 \text{ \AA}$) in line with previous literature[14], eventually splitting up into 4.7 eV (LUMO+1) and 4.5 eV (LUMO) for $d < 3 \text{ \AA}$ due to exchange interactions rising with inverse inter-atomic distance (with the overlap integral of associated orbitals forming a bond). This is another indication that the OH group acts as a "bridge" between CO₂ and Au in terms of electronic coupling, which can then enable electron transfer from a considerably larger distance.

The total DOS of the different systems is shown in Figure S2. The introduction of CO₂ and OH induces only minor alterations in the total DOS due to the dominant contribution of states originating from the Au cluster. Notably, in the presence of the molecules, the Au cluster exhibits a slightly positive charge, which becomes more pronounced when the OH group is involved. The shift of the HOMO to higher energy is $\sim 0.1 \text{ eV}$ for Au+CO₂ (red curve) and $\sim 0.16 \text{ eV}$ for Au+CO₂+OH (green curve). This indicates that both the adsorbed OH and the CO₂ attract negative charges from the Au nanoparticle, as becomes apparent when comparing electronegativities, ionization energies, and electron affinities of C and O vs. Au [58]. Consequently, an electron transfer should occur from the Au NP to the molecular species. The CO₂ molecule induces a significantly increased shift of the HOMO to higher binding energy as compared to the shift when the OH group is included in the system. This dominant energy shift due to the CO₂ molecule suggests that an electron transfer from the Au cluster will eventually reside with the CO₂ molecule rather than with the OH group, the latter presenting merely a transient charge path for transferring an electron to the CO₂ molecule.

Plasmon dynamics and hot electron (HE) generation

We now study the time evolution of the Au, Au + CO₂ and Au + CO₂ systems under light illumination; when present, CO₂ is placed at a distance of 2 \AA from the Au surface. First, the photo absorption spectra of the system are calculated by applying an initial Dirac pulse (δ -kick) in the linear-response regime along the z-direction (and perpendicular to the CO₂ molecule, when present). As the Fourier transform of the δ -kick contains all frequencies with equal proportion, this kick equally excites all the optically allowed transitions and allows us to extract the photoabsorption spectrum. Next, we analyse the energy evolution of the systems after excitation with ultra-short optical pulses at the plasmonic resonance energy, which allows us to calculate the energy distribution of hot carriers generated by the decay of the plasmon. This analysis allows us to estimate the plasmon dephasing time after which most of the energy has been transferred to hot carriers.

The photoabsorption spectra (Fig 3a) are characterized by a smoothly growing intensity starting at around 1 eV, with a plasmon peak at ~ 2.5 eV, followed by a wide modulation up to 4 eV. As expected, the plasmon peak is relatively weak, in line with previous theoretical works on small gold clusters[59-61] which showed that a clear plasmon emerges only when the cluster size exceeds 2 nm[62]. For the combined systems, we observe a slight red-shift (green and red curves in Fig. 3a) of the plasmon peak from 2.66 eV for the single Au cluster, to 2.56 eV and 2.52 eV for Au + CO₂ Au + CO₂ + OH, respectively. This indicates the presence of additional decay channels for the plasmon due to formation of hybridized cluster-molecule states.

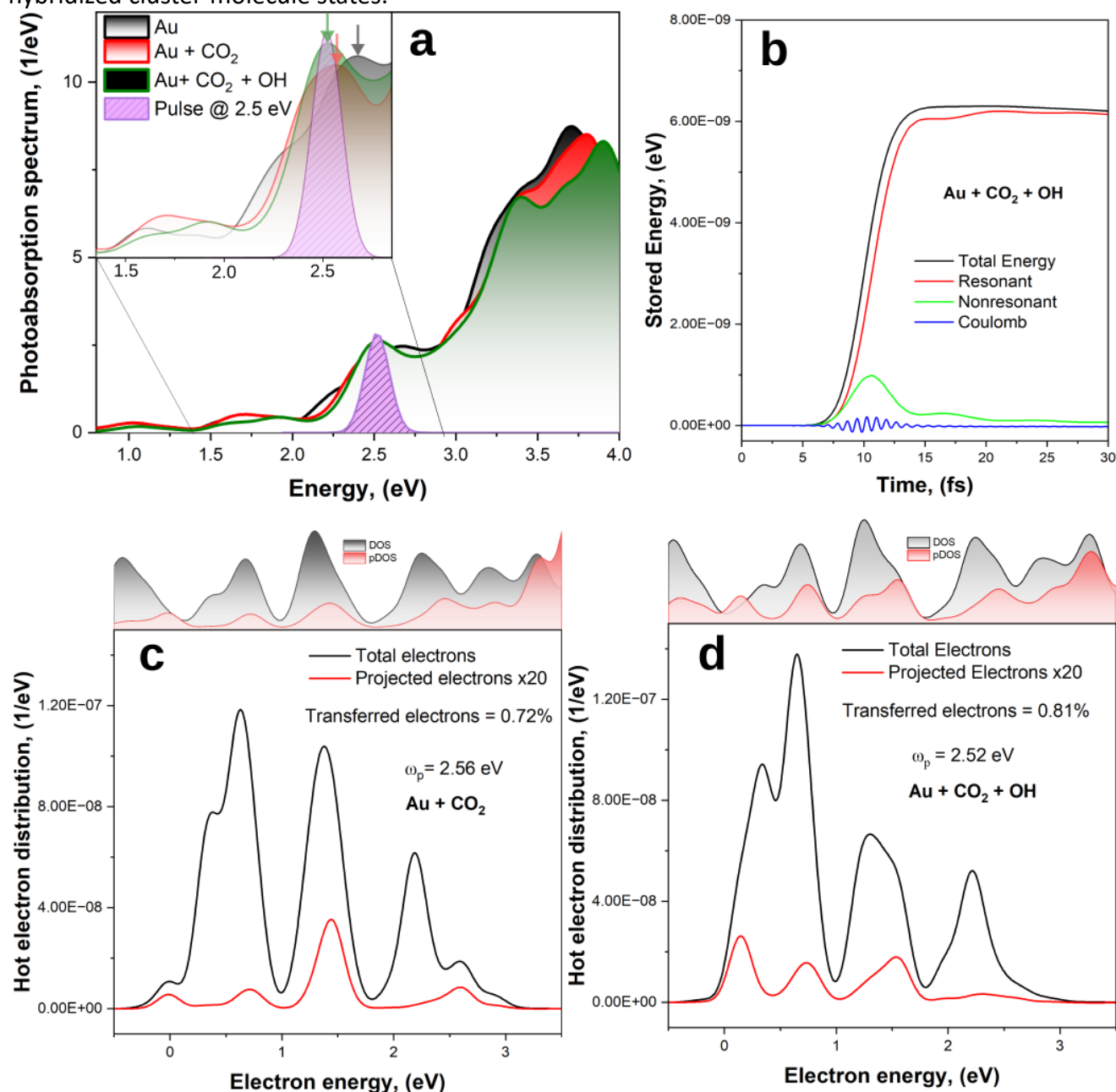


Figure 3. a) Photoabsorption spectra of Au, Au + CO₂ and Au + CO₂ + OH. The purple curve represents a typical driving laser pulse in the frequency domain, centered at the LSPR of the Au + CO₂ + OH. The colour coded arrows represent the LSPR of the different systems. b) Time evolution of the stored energy for Au + CO₂ + OH, highlighting the different energy contributions. c-d) Generated and transferred HEs energy distribution for the Au + CO₂ and Au + CO₂ + OH systems, respectively, averaged between 15 and 30 fs.

Next, we excite the systems with a Gaussian pulse – $E(t) = E_0 \cos(\omega_p(t - t_0))\exp(-\sigma^2(t - t_0)^2/2)$ – with ω_p set to be in resonance with the systems ($\omega_p = 2.66$ eV for Au, 2.56 eV for Au + CO₂ and 2.52 eV for Au + CO₂ + OH), centred at 10 fs and with a temporal FWHM of 5 fs (Fig3 a, purple peak).

The energy of the light pulse is absorbed by the electrons in the system, promoting them into excited states. The electronic energy is not equally distributed, and can be divided into Coulomb energy, and

electron–hole transition energy contributions[41, 63] as shown for the Au + OH + CO₂ system in Fig. 3b. The latter can be further separated into the energy of transitions resonant with the excitation pulse (i.e. with frequency $\omega = \omega_p \pm 2\sigma$), constituting hot carriers, and non-resonant transitions, attributed to transitions from d-states in the metal nanoparticle which screen the plasmon. The evolution of the different energy contributions is similar for all the investigated systems (Fig S3), as the plasmon dephasing process is not affected on a significant scale by a single molecular species. Initially, the plasmon is excited via Coulomb interactions[64] and non-resonant contributions carry most of the energy during the plasmon excitation. After ~ 15 fs, as the plasmon decays, the total energy is redistributed into electron–hole excitations that are resonant with the pulse.

Having established that after ~ 15 fs the energy of the plasmon is mostly stored in hot carriers, we proceed to analyse the energy distribution of the photogenerated HEs, as well as the fraction of such HEs directly excited to states localised on the CO₂ molecule for the Au + CO₂ and Au + CO₂ + OH systems. The HE energy distributions are shown in Fig. 3c-d, where we have averaged the energies of the HEs between 15 fs and 30 fs as the resonant transitions have already reached their steady state. Therefore, HEs possess one temperature in accord with Fermi-Dirac statistics relative to the energy of their steady state as given by the convolution of the initial HE population with the total DOS of the system in the relevant energy range. For both the analysed systems, the generated HEs (black lines) can have energies up to the laser pulse frequency ($E_F + \hbar\omega_p$) due to the energy conservation. In addition, their energy distributions are not uniform within this range but show occupation probabilities that match the total DOS of the systems; electrons can only be excited to existing unoccupied states. The total DOS for Au + CO₂ and Au + CO₂ + OH are similar as they are dominated by the Au contributions. It follows that all systems have similar total HE energy distributions, presenting major peaks at ~ 0.7 eV, 1.3 eV and 2.2 eV.

Conversely, the transferred electron energy distributions (red lines), which represent the fraction of HEs directly excited to states localised on the CO₂, mirror the pDOS and exhibit differences between the systems. Specifically, in absence of the OH group, the fraction of HEs generated on the CO₂ is 0.72%, with most of them having an energy of 1.4 eV. The addition of the OH group increases the density of electronic states (see also Fig. 2b,) thus opening more channels for electron transfer and effectively improving the charge transfer to 0.81%, which corresponds to an 11% increase with respect to the case without OH.

In the next section, we investigate the effect of the excitation parameters –pulse frequency (ω_p) and width (FWHM)– on the direct excitation of HEs to CO₂ orbitals, by varying ω_p from 1.6 eV to 2.8 eV, and the FWHM from 4 fs (1.03 eV) to 15 fs (0.28 eV). The energy distributions of the HEs excited to states localised on the CO₂ molecule are reported in Fig. 4a-d as a function of pulse energy; the distributions for the total amount of HEs in both systems are given in Fig. S4. The amount of generated HEs increases with the increase of pulse width. For FWHM = 4 fs, we obtain a maximum HE density when $\omega_p \sim 2.8$ eV, while for FWHM = 15 fs the maximum occurs when $2.3 < \omega_p < 2.7$ eV for all systems. In this energy range, the pulse excitation approaches the plasmon resonance of the systems (Fig. 3a), thus emphasizing the critical role of spectral overlap in efficiently modulating electron transfer processes[65, 66]. Furthermore, below ~ 2 eV, photoabsorption decreases, thus resulting in a negligible generation of HEs within the molecule. This finding suggests that engineering the photoabsorption, i.e. the plasmon resonance energy, should be considered to efficiently leverage photogenerated HEs for tailored reactions.

In the absence of the OH group (Fig. 4a,c), the energy distribution of HEs exhibits a prominent, dominant single peak centred around ~ 1.4 eV for pulse energies of 2.4-2.6 eV. Notably, approximately

55% (75%) of the HEs assume this specific energy level when subjected to pulse durations with FWHM of 4 fs (15 fs) and under resonance conditions. Conversely, the presence of the OH group results in a broader electron energy distribution. This is attributed to the presence of more accessible hybridized states within the energy range of 0 eV – 2 eV, which can be populated by HEs. The broadened energy distribution as facilitated by the OH group provides more channels for HEs transfer and promotes the system to a different excited level, potentially leading to a different product distribution[6]. This demonstrates that the presence of the OH group in the CO₂ photoreduction process alters the energy landscape and transfer behaviour of HEs, thereby possibly affecting the reaction pathway, and highlight the importance of taking into account the influence of environmental and intermediate species for selective HE catalysis.

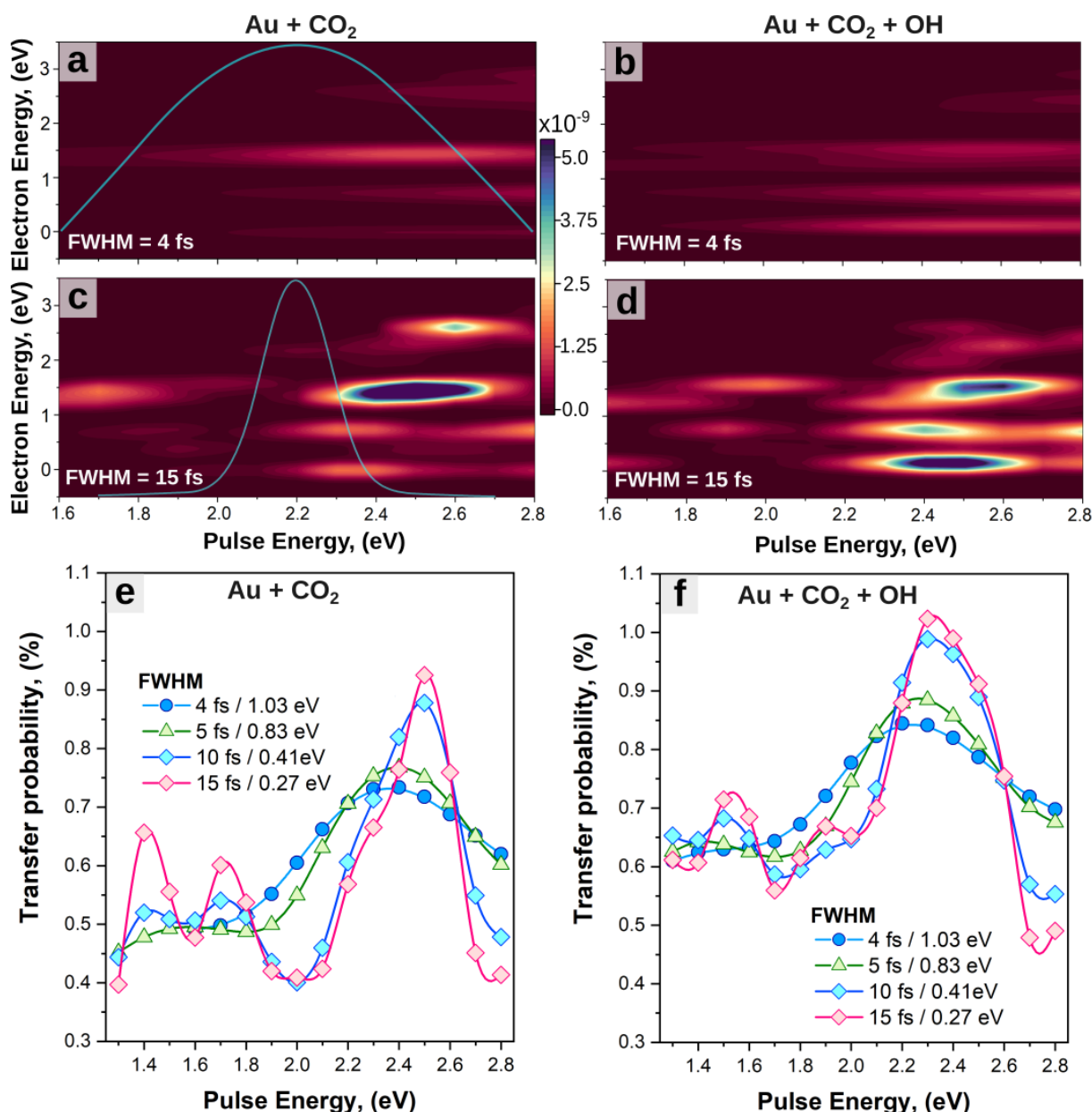


Figure 4. a, b) Amount of HEs generated on CO₂ and their energy distribution as a function of the pulse frequency (with temporal FWHM of 4 fs (1.03 eV)) for Au + CO₂ and Au + CO₂ + OH, respectively. c-d) Same as a-b, but the excitation has a FWHM of 15 fs (0.27 eV). The light blue lines in a) and c) represent a typical laser pulse in frequency domain. e-f) Fraction of carriers that are being transferred to the molecule as a function of the excitation frequency for multiple FWHM.

Furthermore, the excitation width also affects the HE distributions. Narrow band pulses (FWHM = 15 fs; $\Delta E = 0.27$ eV) lead to an overall increase in the generation of HEs on the molecule; conversely, with

'broadband' excitation (FWHM = 4 fs; $\Delta E = 1.03$ eV) the pulse energy is redistributed to a wider range of possible transitions in the photoabsorption spectrum, leading to a broader but less intense (less resonant) electron transfer. The transfer probability is given in Fig. 4 3-f, calculated as the ratio of the number of HEs generated on the molecule to the total HEs in the systems, and exhibits consistently higher values when the OH group is present, indicating a more efficient transfer. Specifically, the addition of the OH group leads to an increase of $\sim 10 - 15\%$ in the transfer probability, depending on pulse frequencies and FWHMs. Interestingly, when transitioning from narrowband to broadband excitation (FWHM = 0.24 eV to 1.03 eV), despite a reduced transfer probability, the electron transfer to acceptor hybridized states remains high, with a maximum probability of ca. 0.84% for Au + CO₂ + OH at $\omega_p = 2.3$ eV. This result suggests that HE transfer can still occur under broadband solar illumination with minor reductions of the yield, which is critical for practical photocatalysts operation.

We note that, while the quantitative results are specific to the systems considered, the fundamental physics elucidated here remains broadly applicable for other systems. Importantly, our findings highlight the critical role of the OH adsorbate in determining (i) the adsorption and activation of CO₂, (ii) the hybridization between Au and CO₂, and (iii) the amount of HEs directly transferred into hybridized states. Consequently, the presence of OH species can promote the CO₂ reduction reaction to a different potential energy surface, possibly leading to different product distributions and reaction speeds. It is therefore very important to consider adsorbed species during the design of plasmonic catalysts to achieve high efficiency and selectivity for specific reactions, particularly when dealing with plasmonic structures functionalized with ligands.

Conclusions

We investigate the mechanisms of plasmon-driven CO₂ reduction in the presence of a co-adsorbed hydroxyl group via real-time time-dependent density functional theory. Our findings show that the OH group induces a redistribution of charges in CO₂, leading to favourable absorption and activation on small Au clusters. Critically, adding an OH group significantly increased hybridization between molecular states of CO₂ and electronic states of Au as mediated by the OH group, enabling and improving charge transfer. This coupling is distance-dependent, with a maximum when the CO₂ is close to the Au cluster, and can be predicted by analysing the branching of the partial density of states of the molecules.

By applying TDDFT, we are able to study the carrier dynamics of these systems at an atomic level, whereby the quantification of the hot electron (HE) energy distribution is critical. While the total HE distribution is largely unaffected by the presence of the OH group, the additional hybridized states facilitate the transfer of HEs to the CO₂ molecule, thereby increasing the resonant direct HE transfer by 11%. Furthermore, our findings confirm the importance of spectral overlap between the excitation energy and the plasmon resonance, and show that direct HE transfer is only slightly decreased ($\sim 1.05\%$ to 0.84%) when the excitation is changed from narrowband to broadband. This finding shows that a significant chemical reaction rate still occurs under broadband excitation such as solar light.

In summary, this investigation elucidates the role of adsorbed hydroxyl groups in the adsorption and activation of CO₂ on plasmonic surfaces. It highlights the importance of considering adsorbed molecules to enhance direct HE transfer, ultimately enabling the design of highly efficient and selective plasmonic photocatalysts with polychromatic excitation.

References

1. Mayer, K.M. and J.H. Hafner, *Localized surface plasmon resonance sensors*. Chem Rev, 2011. **111**(6): p. 3828-57.
2. Fusco, Z., et al., *Nanostructured Dielectric Fractals on Resonant Plasmonic Metasurfaces for Selective and Sensitive Optical Sensing of Volatile Compounds*. Advanced Materials, 2018. **30**(30): p. 1800931.
3. Fusco, Z., et al., *Photonic Fractal Metamaterials: A Metal–Semiconductor Platform with Enhanced Volatile-Compound Sensing Performance*. Advanced Materials, 2020. **32**(50): p. 2002471.
4. Fusco, Z., et al., *Self-assembly of Au nano-islands with tuneable organized disorder for highly sensitive SERS*. Journal of Materials Chemistry C, 2019. **7**(21): p. 6308-6316.
5. Langer, J., et al., *Present and Future of Surface-Enhanced Raman Scattering*. ACS Nano, 2020. **14**(1): p. 28-117.
6. Gargiulo, J., et al., *From Optical to Chemical Hot Spots in Plasmonics*. Acc Chem Res, 2019. **52**(9): p. 2525-2535.
7. Tran-Phu, T., et al., *Multifunctional nanostructures of Au–Bi₂O₃ fractals for CO₂ reduction and optical sensing*. Journal of Materials Chemistry A, 2020. **8**(22): p. 11233-11245.
8. DuChene, J.S., et al., *Hot Hole Collection and Photoelectrochemical CO(2) Reduction with Plasmonic Au/p-GaN Photocathodes*. Nano Lett, 2018. **18**(4): p. 2545-2550.
9. König, D., et al., *Non-equilibrium dynamics, materials and structures for hot carrier solar cells: a detailed review*. Semiconductor Science and Technology, 2020. **35**(7).
10. Zhou, L., et al., *Quantifying hot carrier and thermal contributions in plasmonic photocatalysis*. Science, 2018. **362**(6410): p. 69-72.
11. Verma, R., R. Belgamwar, and V. Polshettiwar, *Plasmonic Photocatalysis for CO₂ Conversion to Chemicals and Fuels*. ACS Materials Letters, 2021. **3**(5): p. 574-598.
12. Zhang, X., et al., *Product selectivity in plasmonic photocatalysis for carbon dioxide hydrogenation*. Nature Communications, 2017. **8**(1): p. 14542.
13. Zhang, Y., et al., *Surface-Plasmon-Driven Hot Electron Photochemistry*. Chem Rev, 2018. **118**(6): p. 2927-2954.
14. Yu, S., et al., *Plasmonic Control of Multi-Electron Transfer and C–C Coupling in Visible-Light-Driven CO₂ Reduction on Au Nanoparticles*. Nano Letters, 2018. **18**(4): p. 2189-2194.
15. Tagliabue, G., et al., *Quantifying the role of surface plasmon excitation and hot carrier transport in plasmonic devices*. Nat Commun, 2018. **9**(1): p. 3394.
16. Liu, T., et al., *Generation of hot electrons in nanostructures incorporating conventional and unconventional plasmonic materials*. Faraday Discuss, 2019. **214**: p. 199-213.
17. Ezendam, S., et al., *Hybrid Plasmonic Nanomaterials for Hydrogen Generation and Carbon Dioxide Reduction*. ACS Energy Lett, 2022. **7**(2): p. 778-815.
18. Yuan, L., et al., *Sustainable chemistry with plasmonic photocatalysts*. 2023. **12**(14): p. 2745-2762.
19. Manjavacas, A., et al., *Plasmon-Induced Hot Carriers in Metallic Nanoparticles*. ACS Nano, 2014. **8**(8): p. 7630-7638.

20. Sundararaman, R., et al., *Theoretical predictions for hot-carrier generation from surface plasmon decay*. Nat Commun, 2014. **5**: p. 5788.
21. Newmeyer, E.-R., J.D. North, and D.F. Swearer, *Hot carrier photochemistry on metal nanoparticles*. Journal of Applied Physics, 2022. **132**(23).
22. Mascaretti, L., et al., *Plasmon-Enhanced Photoelectrochemical Water Splitting for Efficient Renewable Energy Storage*. Adv Mater, 2019. **31**(31): p. e1805513.
23. Mukherjee, S., et al., *Hot-Electron-Induced Dissociation of H₂ on Gold Nanoparticles Supported on SiO₂*. Journal of the American Chemical Society, 2014. **136**(1): p. 64-67.
24. Swaminathan, S., et al., *The Pivotal Role of Hot Carriers in Plasmonic Catalysis of C–N Bond Forming Reaction of Amines*. Angewandte Chemie International Edition, 2021. **60**(22): p. 12532-12538.
25. Yu, S. and P.K. Jain, *Plasmonic photosynthesis of C(1)-C(3) hydrocarbons from carbon dioxide assisted by an ionic liquid*. Nat Commun, 2019. **10**(1): p. 2022.
26. Boerigter, C., et al., *Evidence and implications of direct charge excitation as the dominant mechanism in plasmon-mediated photocatalysis*. Nature Communications, 2016. **7**(1): p. 10545.
27. Kazuma, E. and Y. Kim, *Mechanistic Studies of Plasmon Chemistry on Metal Catalysts*. Angewandte Chemie International Edition, 2019. **58**(15): p. 4800-4808.
28. Chen, K. and H. Wang, *Plasmon-driven photocatalytic molecular transformations on metallic nanostructure surfaces: mechanistic insights gained from plasmon-enhanced Raman spectroscopy*. Molecular Systems Design & Engineering, 2021. **6**(4): p. 250-280.
29. Kumar, P.V., et al., *Direct hot-carrier transfer in plasmonic catalysis*. Faraday Discuss, 2019. **214**: p. 189-197.
30. Sun, Y. and Z. Tang, *Photocatalytic hot-carrier chemistry*. MRS Bulletin, 2020. **45**(1): p. 20-25.
31. Yu, S., et al., *Opportunities and Challenges of Solar-Energy-Driven Carbon Dioxide to Fuel Conversion with Plasmonic Catalysts*. ACS Energy Letters, 2017. **2**(9): p. 2058-2070.
32. Wu, Y., et al., *SERS Study of the Mechanism of Plasmon-Driven Hot Electron Transfer between Gold Nanoparticles and PCBM*. The Journal of Physical Chemistry C, 2019. **123**(49): p. 29908-29915.
33. Le, T., Y. Shao, and B. Wang, *Plasmon-Induced CO₂ Conversion on Al@Cu₂O: A DFT Study*. The Journal of Physical Chemistry C, 2021. **125**(11): p. 6108-6115.
34. Sandoval, M.G., et al., *CO₂ adsorption and activation on Ag(111) surfaces in the presence of surface charge density: A static gas phase DFT study*. Applied Surface Science, 2023. **610**: p. 155498.
35. Hu, C., et al., *Near-infrared-featured broadband CO₂ reduction with water to hydrocarbons by surface plasmon*. Nature Communications, 2023. **14**(1): p. 221.
36. Zhang, X.-G., et al., *Reaction Selectivity for Plasmon-Driven Carbon Dioxide Reduction on Silver Clusters: A Theoretical Prediction*. The Journal of Physical Chemistry C, 2019. **123**(17): p. 11101-11108.
37. Xiong, Y., et al., *Photodriven Catalytic Hydrogenation of CO₂ to CH₄ with Nearly 100% Selectivity over Ag₂₅ Clusters*. Nano Letters, 2021. **21**(20): p. 8693-8700.
38. Yan, J., K.W. Jacobsen, and K.S. Thygesen, *First-principles study of surface plasmons on Ag(111) and H/Ag(111)*. Physical Review B, 2011. **84**(23): p. 235430.
39. Rossi, T.P., et al., *Kohn-Sham Decomposition in Real-Time Time-Dependent Density-Functional Theory: An Efficient Tool for Analyzing Plasmonic Excitations*. J Chem Theory Comput, 2017. **13**(10): p. 4779-4790.
40. Kumar, P.V., et al., *Plasmon-Induced Direct Hot-Carrier Transfer at Metal-Acceptor Interfaces*. ACS Nano, 2019. **13**(3): p. 3188-3195.
41. Rossi, T.P., P. Erhart, and M. Kuisma, *Hot-Carrier Generation in Plasmonic Nanoparticles: The Importance of Atomic Structure*. ACS Nano, 2020. **14**(8): p. 9963-9971.

42. Fojt, J., et al., *Hot-Carrier Transfer across a Nanoparticle–Molecule Junction: The Importance of Orbital Hybridization and Level Alignment*. *Nano Letters*, 2022. **22**(21): p. 8786-8792.
43. Kuisma, M., et al., *Localized surface plasmon resonance in silver nanoparticles: Atomistic first-principles time-dependent density-functional theory calculations*. *Physical Review B*, 2015. **91**(11): p. 115431.
44. Zhu, W., et al., *Monodisperse Au Nanoparticles for Selective Electrocatalytic Reduction of CO₂ to CO*. *Journal of the American Chemical Society*, 2013. **135**(45): p. 16833-16836.
45. Gao, D., et al., *Enhancing CO₂ Electroreduction with the Metal–Oxide Interface*. *Journal of the American Chemical Society*, 2017. **139**(16): p. 5652-5655.
46. Lee, J.H., et al., *Understanding the Role of Functional Groups in Polymeric Binder for Electrochemical Carbon Dioxide Reduction on Gold Nanoparticles*. *Advanced Functional Materials*, 2018. **28**(45).
47. Sun, M., A. Staykov, and M. Yamauchi, *Understanding the Roles of Hydroxide in CO₂ Electroreduction on a Cu Electrode for Achieving Variable Selectivity*. *ACS Catalysis*, 2022. **12**(24): p. 14856-14863.
48. Deng, W., et al., *Crucial Role of Surface Hydroxyls on the Activity and Stability in Electrochemical CO₂ Reduction*. *Journal of the American Chemical Society*, 2019. **141**(7): p. 2911-2915.
49. Singh, S., et al., *Surface plasmon-enhanced photo-driven CO₂ hydrogenation by hydroxy-terminated nickel nitride nanosheets*. *Nature Communications*, 2023. **14**(1): p. 2551.
50. Vu, N.N., S. Kaliaguine, and T.O. Do, *Plasmonic Photocatalysts for Sunlight-Driven Reduction of CO(2) : Details, Developments, and Perspectives*. *ChemSusChem*, 2020. **13**(16): p. 3967-3991.
51. Álvarez, A., et al., *CO₂ Activation over Catalytic Surfaces*. *ChemPhysChem*, 2017. **18**(22): p. 3135-3141.
52. Cohen, K.Y., et al., *Using Light and Electrons to Bend Carbon Dioxide: Developing and Understanding Catalysts for CO₂ Conversion to Fuels and Feedstocks*. *Accounts of Chemical Research*, 2022. **55**(7): p. 944-954.
53. Zhu, S., et al., *A computational study on linear and bent adsorption of CO₂ on different surfaces for its photoreduction*. *Catalysis Today*, 2019. **335**: p. 278-285.
54. Cheng, D., R. Liu, and K. Hu, *Gold nanoclusters: Photophysical properties and photocatalytic applications*. *Front Chem*, 2022. **10**: p. 958626.
55. Pyykko, P. and J.P. Desclaux, *Relativity and the periodic system of elements*. *Accounts of Chemical Research*, 1979. **12**(8): p. 276-281.
56. Meyer, R., et al., *Surface chemistry of catalysis by gold*. *Gold Bulletin*, 2004. **37**(1): p. 72-124.
57. Tao, Z., et al., *Bridge Sites of Au Surfaces Are Active for Electrocatalytic CO₂ Reduction*. *Journal of the American Chemical Society*, 2022. **144**(19): p. 8641-8648.
58. Wiberg, E.W.N., and A F. Holleman, *Inorganic Chemistry*. 2001, San Diego: Academic Press.
59. Baseggio, O., et al., *Photoabsorption of Icosahedral Noble Metal Clusters: An Efficient TDDFT Approach to Large-Scale Systems*. *The Journal of Physical Chemistry C*, 2016. **120**(23): p. 12773-12782.
60. Iida, K., et al., *First-Principles Computational Visualization of Localized Surface Plasmon Resonance in Gold Nanoclusters*. *The Journal of Physical Chemistry A*, 2014. **118**(47): p. 11317-11322.
61. Durante, N., et al., *Optical Properties of Au Nanoclusters from TD-DFT Calculations*. *The Journal of Physical Chemistry C*, 2011. **115**(14): p. 6277-6282.
62. Piccini, G., et al., *Gold Nanowires: A Time-Dependent Density Functional Assessment of Plasmonic Behavior*. *The Journal of Physical Chemistry C*, 2013. **117**(33): p. 17196-17204.
63. Kluczyk-Korch, K. and T.J. Antosiewicz, *Hot carrier generation in a strongly coupled molecule–plasmonic nanoparticle system*. *Nanophotonics*, 2023. **0**(0).
64. Ma, J., Z. Wang, and L.-W. Wang, *Interplay between plasmon and single-particle excitations in a metal nanocluster*. *Nature Communications*, 2015. **6**(1): p. 10107.

65. Fusco, Z., K. Catchpole, and F.J. Beck, *Investigation of the mechanisms of plasmon-mediated photocatalysis: synergistic contribution of near-field and charge transfer effects*. *Journal of Materials Chemistry C*, 2022. **10**(19): p. 7511-7524.
66. Fusco, Z., et al., *Cathodoluminescence Spectroscopy of Complex Dendritic Au Architectures for Application in Plasmon-Mediated Photocatalysis and as SERS Substrates*. *Advanced Materials Interfaces*, 2023. **10**(3): p. 2202236.